Ballistic Equivalent Thickness Analytical Theory for Ductile-Hole-Growth Metal Targets Penetrated by Ogive-Nose Armor-Piercing Projectiles

Tao Li[a], WenJin Yao[a*], Wei Zhu[a],Wenbin Li[a]

[a]School of Mechanical Engineering, Nanjing University of Science and Technology; Nanjing, China. Email: litaolitao@njust.edu.cn , njyaowj@163.com , 12021059@njust.edu.cn , lwb2000cn@njust.edu.cn.

* Corresponding author

Abstract

Ballistic equivalent thickness calculation is a key bottleneck in armor lightweight design and penetration damage evaluation. Traditional fixed strength ratio and curve-fitting methods ignore coupled energy dissipation and plastic hardening during penetration, leading to large conversion errors across diverse projectile working conditions. While cavity expansion theory accurately predicts ballistic limit velocity, inverse derivation for ballistic equivalence between dissimilar targets remains unexplored. This work conducts strict mathematical inversion via compressible cavity expansion theory to establish an explicit analytical formula of ballistic equivalent thickness for ductile metal targets penetrated by ogive-nose armor-piercing projectiles. Model validation is carried out using over 950 independent penetration equivalence cases from a public authoritative ballistic dataset, without any empirical calibration. The proposed model yields a mean absolute percentage error of only 7.4% for ductile hole-growth metals, far outperforming conventional empirical power-law models in prediction precision and relevance. Theoretical analysis proves that when inertial effects are negligible, the equivalent thickness ratio of two ductile metallic targets depends exclusively on their quasi-static cavity expansion resistance, independent of projectile geometry, density, mass and other parameters. The derived conversion formula removes the need for repeated experimental calibration in traditional schemes. It provides a traceable theoretical basis for quantitative armor material matching and lightweight protective structural design, and supports equivalent substitution tests and engineering optimization of armored vehicle and warship protective panels.

Keywords

Cavity expansion theory, Ballistic equivalence, Equivalent thickness, Ballistic limit velocity

Graphical Abstract

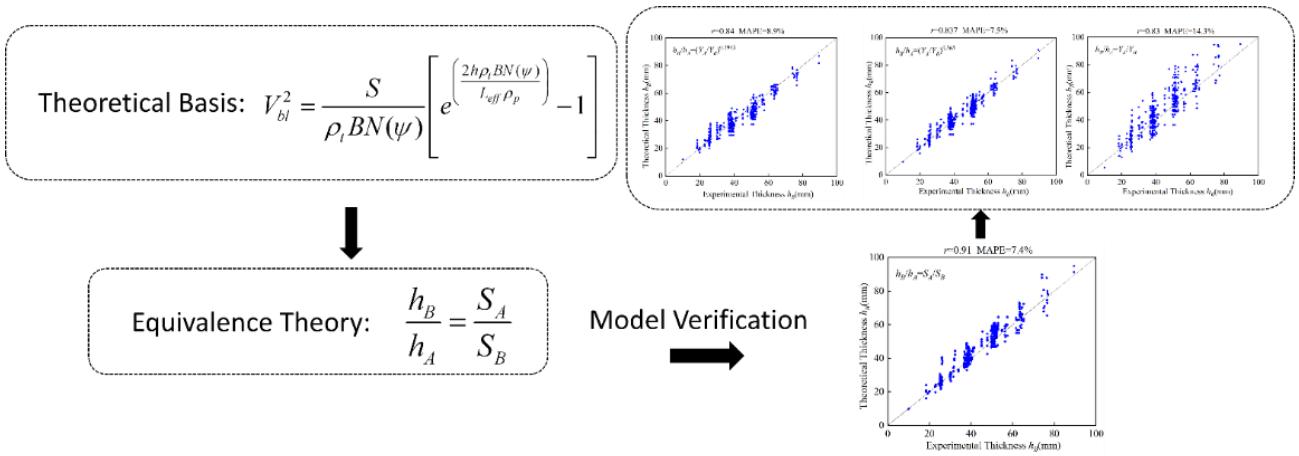

1 INTRODUCTION

In the fields of armor structural optimization and terminal ballistic damage assessment, the ballistic equivalence problem of targets under projectile-target interaction is a fundamental research topic of considerable engineering importance, as it enables the equivalent replacement of ballistic performance across targets of different materials and thicknesses (Bishop et al., 1945; Masri, 2015; Masri and Ryan, 2023; Qi et al., 2024). Lightweight armor design, selection of novel protective materials, and equivalent scaling in sub-scale model tests all rely on accurate ballistic thickness equivalence relationships. An excessive deviation in equivalent thickness determination can directly lead to either redundant overdesign or insufficient protection, severely compromising both protection effectiveness and cost-efficiency. Consequently, establishing an analytical theory of ballistic equivalence that possesses clear physical mechanisms, can be generalized across operating conditions, and requires no empirical calibration is the core foundation for refined armor engineering.

Current engineering practice in armor target equivalence conversion is dominated by empirical fitting and numerical simulation fitting methods, which inherently suffer from ambiguous physical meaning, poor extrapolability, and dependence on case-specific calibration. The classical fixed strength-ratio conversion method, widely adopted in armor design handbooks, is computationally simple but neglects plastic hardening and differences in dynamic resistance of materials, resulting in extremely limited adaptability. The Lambert-Jonas empirical power-law model (Lambert and Jonas, 1976) is a mainstream tool for ballistic data analysis; however, its fitting parameters lack physical interpretability and cannot provide extrapolative predictions for equivalence conversion between different projectile-target combinations. Han and Jiang (2023) proposed a thickness equivalent model for plates of different materials based on the similarity of projectile residual velocity, but the model still requires physical tests to calibrate simulation parameters. Wang et al. (2023) established a material similarity framework that enables targets made of different materials to be applied to penetration problems. Because differences in fracture toughness can lead to incomplete similarity, they introduced the concepts of volumetric failure strain and volumetric yield stress, which can effectively describe high-velocity penetration problems involving fracture toughness; nevertheless, the model is complex and not well suited to engineering application. Mullin et al. (2003) developed a velocity scaling method for dissimilar materials in the hypervelocity impact regime, extrapolating results from scaled tests to prototype conditions through similarity relations of material density and strength. Du et al. (2025a) proposed a comparison method for impact equivalence, a novel approach to evaluating the equivalence of impact energy for metals and composites, that can achieve mutual equivalence between different materials, although it remains fundamentally based on fitting to experimental data. The classical scaling laws of Wen and Jones (1993) have provided a rigorous theoretical foundation for sub-scale tests of similar materials, but they do not resolve the issue of equivalence between different material classes. Du et al. (2025b) established two equivalence criteria for composite laminates, ballistic limit equivalence and equal energy equivalence, based on the Lambert-Jonas equation and the condition of equal energy.

Cavity expansion theory (CET) is one of the most physically rigorous analytical frameworks in terminal ballistics. Its theoretical roots can be traced to the plastic analysis of hardness tests by Bishop, Hill and Mott (Bishop et al., 1945), which laid the conceptual foundation of CET. Hill (1998) presented an expression for the quasi-static expansion resistance of an incompressible spherical cavity in the mathematical theory of plasticity. Forrestal and Luk (1988) introduced material compressibility into the spherical cavity expansion framework, and subsequently Luk et al. (1991) further incorporated power-law strain hardening, establishing a resistance calculation system applicable to a broader range of material constitutive relations. Forrestal et al. (1990) were the first to successfully apply CET to the V_{50} prediction of conical-nose projectiles perforating aluminum alloy targets; Warren and Forrestal (1998) extended this framework to spherical-nose projectile configurations; Forrestal and Warren (2009) provided unified analytical formulas for residual velocity covering both conical and ogival rigid projectiles, but they did not go further to derive equivalent conversion relationships for targets.

The main contributions of this paper are as follows:

Based on the classical cavity expansion V_{bl} prediction model, with ballistic limit velocity equivalence as the constraint condition, the closed-form analytical derivation of equivalent thickness is completed; multi-dimensional model validation is conducted using 950 pairs of experimental data, quantifying prediction accuracy and systematic bias; the root causes of model accuracy, approximation conditions, and applicability range are deeply analyzed, and accuracy benchmarking against conventional equivalent methods is performed; the model failure mechanisms and operational boundaries are clarified, and the core research conclusions are distilled.

2 THEORETICAL MODEL DERIVATION

2.1 Basic Assumptions

This paper focuses on the penetration condition of ductile-hole-growth metallic target plates under normal impact by ogive-nose rigid armor-piercing projectiles. To ensure the physical rigor of the theoretical derivation and in conjunction with the fundamental framework of cavity expansion theory, the following basic assumptions are established, with their rationality justified:

(1) The target plate material is homogeneous, isotropic, and ductile-hole-growth metal, exhibiting deformation behavior consistent with power-law strain hardening, free from initial defects and anisotropy, which conforms to the mechanical characteristics of conventional armor metallic materials.

(2) The projectile is rigid, undergoing no deformation, erosion, fragmentation, or mass loss during penetration. This assumption is satisfied under conventional high-strength ogive-nose armor-piercing projectile penetration of metallic target plates.

(3) During penetration, the normal stress is separable and superposable. The plastic hole-growth deformation of the target plate conforms to the stress distribution and deformation assumptions of cavity expansion theory, representing a classical mechanical prerequisite for ductile-hole-growth penetration.

(4) The target plate failure mode is uniform ductile hole-growth. The model is not applicable to non-ductile-hole-growth conditions such as adiabatic shear plugging failure for blunt-nose projectiles or three-dimensional complex contact failure for spherical projectiles, establishing a clear applicability boundary of the failure mechanism for the model.

(5) Projectile-target interface friction effects are neglected. Mechanical magnitude analysis indicates that during ductile-hole-growth penetration, the frictional resistance at the projectile-target interface constitutes less than 5% of the cavity plastic resistance, exerting a negligible influence on the overall penetration dynamic response and can be safely ignored.

2.2 Closed-Form Analytical Derivation of Equivalent Thickness

This paper conducts the inverse derivation of ballistic equivalent thickness based on the Forrestal-Warren (2009) rigid projectile penetration cavity expansion theory mode. The classical formula for calculating the ballistic limit velocity is as follows:

$$V_{bl}^2 = \frac{S}{\rho_t BN(\psi)}\left[e^{\left(\frac{2h\rho_t BN(\psi)}{L_{eff}\rho_p}\right)} - 1\right] \tag{1}$$

Where V_{bl} is the ballistic limit perforation velocity of the target plate; ρ_t is the density of the target plate material; h is the target plate thickness; ρ_p is the projectile density; L_{eff} is the effective length of the projectile; S is the quasi-static cavity expansion resistance, a core parameter comprehensively characterizing the material's resistance to plastic deformation; B is the dynamic inertia term constant; ψ is the projectile nose CRH (caliber-radius-head) shape parameter; $N(\psi)$ is the ogive-nose inertial efficiency coefficient, characterizing the influence of projectile nose configuration on penetration dynamics.

The quasi-static cavity expansion stress S is obtained through comprehensive integration of material yield strength, elastic modulus, Poisson's ratio, and strain hardening exponent. The complete expression is:

$$\begin{cases} S = \dfrac{Y}{\sqrt{3}}\left[1 + \left(\dfrac{E}{\sqrt{3}Y}\right)^n \int_0^b \dfrac{(-\ln x)^n}{1-x}dx\right] \\ b = 1 - \dfrac{2(1+\nu)Y}{\sqrt{3E}} \end{cases} \tag{2}$$

where Y is the yield strength of the target plate, n is the plastic strain hardening coefficient, ν is the Poisson's ratio of the target plate material, and E is the elastic modulus. This parameter integrates the plastic flow characteristics of the material throughout the entire process from yielding to perforation, providing a comprehensive characterization of the material's penetration resistance and overcoming the limitations of the single yield strength parameter.

The formula for calculating the projectile nose inertial efficiency coefficient is:

$$N(\psi) = 8\psi^2 \ln\left(\frac{2\psi}{2\psi - 1}\right) - (1 + 4\psi) \tag{3}$$

To simplify the derivation, the equivalent structural parameter for material *i* is defined as:

$$\Lambda_i \equiv \frac{2}{L_{\text{eff}}\rho_p}\rho_{t,i}B_{0,i}N(\psi), \quad i \in \{A,B\} \tag{4}$$

For a given rigid projectile, a target plate $T_A(h_A)$ made of material A with thickness h_A and a target plate $T_B(h_B)$ made of material B with thickness h_B are defined as ballistically equivalent if and only if they exhibit exactly the same ballistic limit velocity for the same projectile, i.e., satisfying:

$$V_{\text{bl}}^{(A)}(h_A) = V_{\text{bl}}^{(B)}(h_B) \tag{5}$$

Substituting the limit velocity formula into the equivalence constraint condition, and noting that $N(\psi)$、L_{eff} and ρ_p are constant for the same projectile, simplification yields:

$$\frac{S_A}{\rho_{t,A}B_A}\left(e^{\Lambda_A h_A}-1\right) = \frac{S_B}{\rho_{t,B}B_B}\left(e^{\Lambda_B h_B}-1\right) \tag{6}$$

Further solving gives the exact explicit solution for the equivalent thickness:

$$h_B = \frac{1}{\Lambda_B}\ln\left[1+\frac{S_A}{S_B}\cdot\frac{\rho_{t,B}B_B}{\rho_{t,A}B_A}\left(e^{\Lambda_A h_A}-1\right)\right] \tag{7}$$

The above exact solution contains parameters such as ρ_t, B_0, L_{eff}, $N(\psi)$ and ρ_p, and there is no publicly available unified method for determining B_0, resulting in poor engineering applicability. When the inertial effect during perforation is much smaller than the quasi-static cavity expansion resistance, a first-order Taylor series expansion approximation of the exponential term can be performed, enabling precise parameter cancellation and simplification:

$$\frac{S_A}{\rho_{t,A}B_A N}\cdot\frac{2\rho_{t,A}B_A N}{\rho_p L_{\text{eff}}}\cdot h_A = \frac{S_B}{\rho_{t,B}B_B N}\cdot\frac{2\rho_{t,B}B_B N}{\rho_p L_{\text{eff}}}\cdot h_B \tag{8}$$

After Taylor expansion, simplification, and cancellation, the projectile density, effective length, nose shape, target plate density, and dynamic inertia constant all cancel out, ultimately yielding the simplified core formula for ballistic equivalent thickness:

$$\frac{h_B}{h_A} = \frac{S_A}{S_B} \tag{9}$$

This formula demonstrates that under conditions dominated by ductile hole-growth with negligible inertial effects, the ballistic equivalent thickness ratio between dissimilar metallic target plates is determined solely by the ratio of the quasi-static cavity expansion resistances of the two materials, independent of projectile geometry, material, and dimensional parameters. The parameter *S* integrates the material yield strength, strain hardening, and elastic properties, serving as the core physical scalar characterizing the penetration resistance of ductile metals against ogive-nose projectiles, requiring no empirical fitting or experimental calibration and being directly computable from basic material mechanical parameters.

3 MODEL VALIDATION

3.1 Data Source

The equivalent model is derived based on the ballistic limit V_{bl}. This paper employs the publicly accessible Mendeley V_{50} database by Ryan et al. (2023) as the benchmark validation set. Conceptually, V_{bl} is a physical threshold whereas V_{50} is a statistical median; however, under ductile-hole-growth conditions, the numerical difference between the two is extremely small, such that equality of V_{50} for two materials can be considered to imply approximate equality of V_{bl}. Thus, V_{50} equivalence is used as a practical surrogate for V_{bl} equivalence. This database consolidates 1084 ballistic limit experimental records from 31 published articles. Each record provides projectile type, geometric parameters, target plate material designation, mechanical property parameters (yield strength *Y*, elastic modulus *E*, Poisson's ratio *v*, density ρ, Ludwik strain hardening exponent *n*), impact angle ϑ, and the experimentally measured V_{50}.The data sources are traceable and of high reliability. To focus on the validation of equivalence under ductile-hole-growth conditions, the following screening criteria are applied: (i) exclusion of blunt-nose fragment-simulating projectiles, which induce shear plugging rather than ductile hole-growth; (ii) exclusion of spherical common projectiles, whose blunt nose geometry violates the ductile-hole-growth assumption and for which the sample size is excessively small; (iii) retention of only normal impact cases (0° incidence angle),as oblique impact would require additional angle correction factors.

After screening, a total of 584 normal impact datasets of AP armor-piercing projectiles are retained, comprising 528 aluminum alloy (Al) target plate datasets and 56 armor steel (St) target plate datasets. Based on the experimental data, the rule for determining equivalent target plate pairs is established as follows: when the same projectile penetrates two different materials, if the difference in their ballistic limit velocities V_{bl} is less than 1%,they are considered actually equal within a 1% tolerance range, and the two plates constitute an experimentally equivalent pair.Ultimately,950 equivalent pairs are obtained, including 724 aluminum-aluminum pairs,210 aluminum-steel pairs, and 16 steel-steel pairs. The cavity expansion resistance S for all tested materials is calculated from the basic material mechanical parameters. The material parameters and S values are summarized in Table 1, and the variation pattern of *S* with yield strength *Y* is shown in Figure 1.

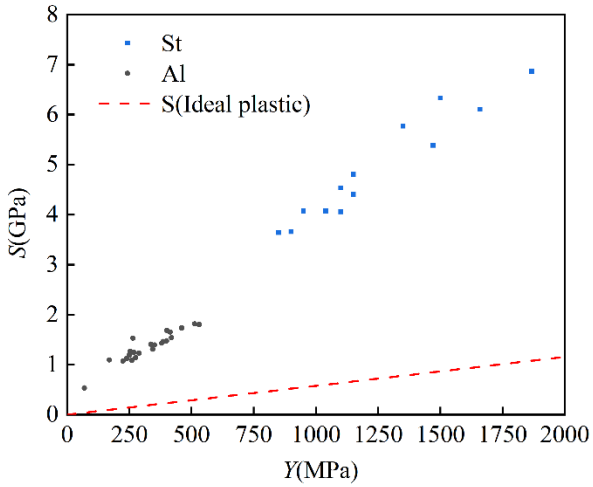

Figure 1 Relationship between quasi-static cavity expansion resistance *S* and material yield strength *Y*.

Table 1 Summary of quasi-static cavity expansion resistance *S* parameters for aluminum and steel materials used in experiments

type	Material	*S*	type	Material	*S*
Al	Al2024-T351	1.529070865	Al	Al7056-T751	1.461208935
Al	Al2060-T8	1.683409312	Al	Al7056-T761	1.803386222
Al	Al2139-T8	1.650049286	Al	Al7075-T651	1.735405888
Al	Al5059-H131	1.265142488	Al	Al7085-T711	1.816553927
Al	Al5059-H136	1.242689688	Al	Al7085-T721	1.537138338
Al	Al5083-H112	1.073536605	Steel	ARMOX370	4.058702012
Al	Al5083-H116	1.123042576	Steel	ARMOX500	5.386202229
Al	Al5083-H131	1.190520955	Steel	ARMOX560	6.104659985
Al	Al6055-T651	1.309471537	Steel	ARMOX600	6.862779896
Al	Al6061-T651	1.138134183	Steel	BISHHA	5.770387464
Al	Al6070-O	0.531490486	Steel	BISHTA	4.534273044
Al	Al6070-T4	1.096282384	Steel	BISRHA300	3.658635836
Al	Al6070-T6	1.394181905	Steel	BISRHA360	4.069097463
Al	Al6070-T7	1.23264287	Steel	BISUHH	6.330613018
Al	Al6082-T6	1.087137463	Steel	BISUHTA	4.802482107
Al	Al7017-T6	1.474171926	Steel	MARS440	4.408189997
Al	Al7017-T7	1.42907614	Steel	SECURE350	3.642941982
Al	Al7039-T64	1.405289439	Steel	SECURE400	4.072631381
Al	Al7056-T721	1.461208935			

Figure 1 and Table 1 demonstrate the relationship curve between quasi-static cavity expansion resistance *S* and yield strength *Y*, as well as the S parameters of the target plate materials. It can be observed that relative to ideal plasticity, *S* can serve as a unified strength indicator characterizing the penetration resistance of ductile metals, clearly reflecting material category, failure mechanism, and equivalent performance differences. Overall, *S* exhibits a significantly monotonic increasing relationship with yield strength *Y*, and can distinguish the ballistic potential of materials under different alloy compositions and heat treatment conditions. The *S* values of aluminum alloys are concentrated in the range of 0.5–1.9, displaying a compact distribution with high linearity, indicating that stable ductile hole-growth dominates under ogive-nose projectile penetration, which is highly consistent with the assumptions of cavity expansion theory. The *S* values of armor steels are generally in the range of 3.6–6.9, significantly higher than those of aluminum alloys, quantitatively confirming that the ballistic resistance of steel is much stronger than that of aluminum at the same

thickness. Moreover, the substantial span and pronounced dispersion of *S* values within steels reveal the transition of failure mode from ductile hole-growth to adiabatic shear localization in high-strength steels.

3.2 Theoretical Validation

For the aluminum-aluminum pairs, totaling 724 samples, all aluminum alloy materials possess a face-centered cubic (FCC) crystal structure. Their high thermal diffusivity ensures that the penetration process is dominated by uniform ductile hole-growth, which is consistent with the theoretical assumptions of this paper. The analytical formula derived in this paper is employed to predict the equivalent thickness, and the results are compared with experimental measured values. The error statistics are presented in Table 2, and the comparison between theory and experiment is shown in Figure 2.

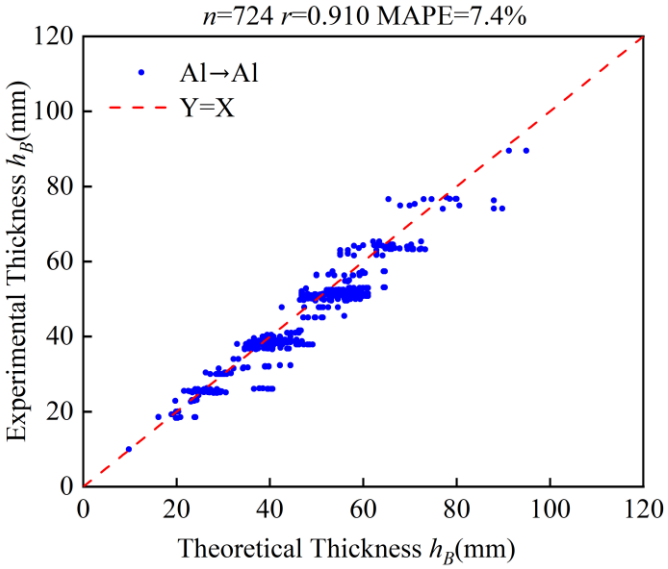

Figure 2 Comparison of theoretical and experimental equivalent thickness values for aluminum-aluminum pairs

Table 2 Statistical results of prediction errors for aluminum-aluminum bidirectional equivalence

Direction	Number of pairs	Mean theoretical ratio	Mean experimental ratio	MAPE	*r*	Bias
h_B/h_A	724	1.177	1.122	7.40%	0.91	5.00%
h_A/h_B	724	0.884	0.922	6.70%	0.91	-4.10%

Table 2 indicates that the correlation coefficient *r*=0.910 demonstrates a highly significant correlation between the cavity expansion resistance ratio *S* and the experimental thickness ratio, with the equivalent trend predicted theoretically being highly consistent with experimental observations. The difference in MAPE between the forward and reverse directions is only 0.7 percentage points, which arises from the denominator effect of percentage error when the predicted ratio deviates from unity, rather than from asymmetry inherent in the formula itself. The positive bias of +5.0% indicates that the theory systematically overestimates the thickness required for material *B* by approximately 5%.This positive bias, being directionally consistent in aluminum-aluminum pairs, originates from the loss of accuracy of the power-law fitting *n* value under extremely high strains in the *S* calculation, as well as the residual systematic deviation in the thick plate regime resulting from the inertial-neglecting approximation.

The error distribution decomposed by material pairs is uniform, with the *S* values corresponding to approach conditions for different heat treatment states of the same alloy. Pairs exhibiting larger errors predominantly involve materials with extremely low *n* values, such as Al7056-T76 (*n*=0.037), for which the power-law hardening integral is highly sensitive to fitting errors when n approaches zero. No systematic correlation is observed between the error and the magnitude of the *S* difference in aluminum-aluminum pairs, indicating that the formula exhibits consistent prediction accuracy for both "similar materials" and "materials with large differences."

For the aluminum-steel pairs, totaling 210 samples, representing mixed failure conditions with ductile hole-growth on one side and a propensity for adiabatic shear on the other, the statistical results of bidirectional conversion errors of the model are presented in Table 3,and the comparison between experiment and theory is shown in Figure 3.The results demonstrate that the MAPE for the aluminum →steel forward conversion is 15.0%,while that for the steel →aluminum reverse conversion is 20.6%.The correlation coefficient *r* for both directions is 0.777,indicating good consistency in the predicted trend.

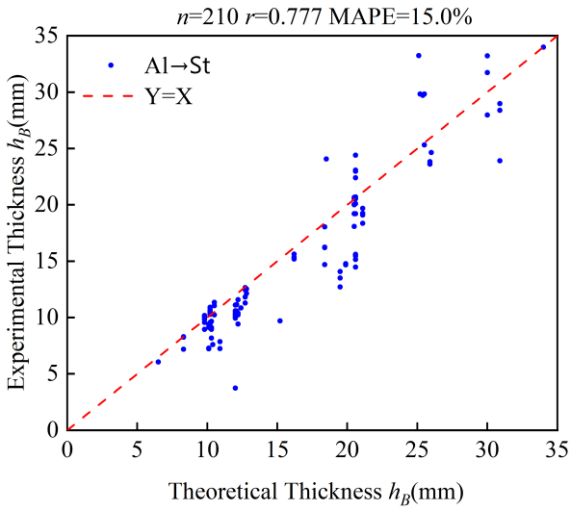

Figure 3 Comparison of theoretical and experimental equivalent thickness values for aluminum-steel pairs

Table 3 Statistical results of prediction errors for aluminum-steel bidirectional equivalence

Direction	Number of pairs	Mean theoretical ratio	Mean experimental ratio	MAPE	*r*	Bias
h_{st}/h_{Al}	210	0.320	0.378	15.00%	0.777	-13.7%
h_{Al}/h_{st}	210	3.125	2.646	20.60%	0.777	+19.65%

Table 3 shows that the difference in bidirectional errors does not arise from model asymmetry but from the denominator effect of percentage errors: for aluminum →steel conversion, using the experimentally measured thickness of steel as the denominator suppresses the error; for steel →aluminum conversion, using the experimentally measured thickness of aluminum as the denominator amplifies the error. From a physical mechanism perspective, the root cause of the error is that high-strength steel is prone to adiabatic shear localization, deviating from the uniform ductile-hole-growth assumption, which renders the *S* parameter incapable of fully characterizing the true penetration resistance of the steel. The theory slightly overestimates the ballistic performance of steel, ultimately resulting in a systematic bias.

The number of valid steel-steel equivalent pairs is only 16. The sample size is limited, and the penetration failure of high-strength armor steel is dominated by adiabatic shear plugging, which completely violates the theoretical assumptions of the model. The validation results are shown in Table.4 and Figure 4. The MAPE for these conditions reaches 24.2%, with a correlation coefficient of only 0.344, indicating extremely poor predictive correlation and complete model failure. This result confirms the core applicability premise of the model in this paper: it is only applicable to penetration conditions dominated by ductile hole-growth, while the equivalent conversion of high-strength steel dominated by shear failure requires a completely new theoretical framework.

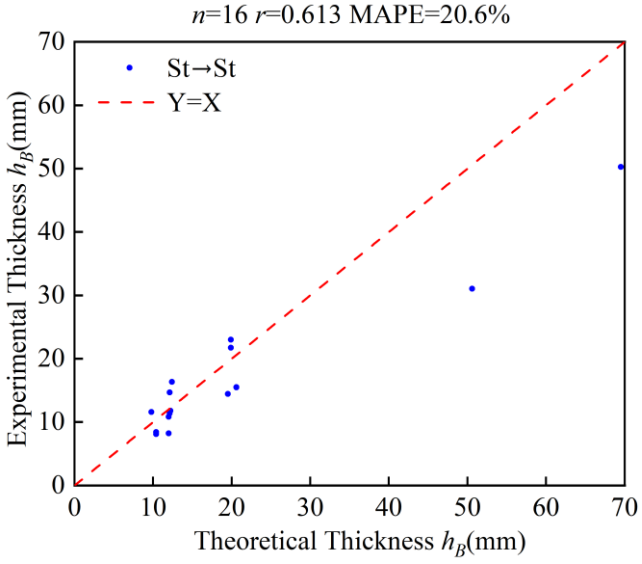

Figure 4 Comparison of theoretical and experimental equivalent thickness values for steel-steel pairs

Table 4 Statistical results of prediction errors for steel-steel bidirectional equivalence

Direction	Number of pairs	MAPE	r	Bias
h_{Al}/h_{st}	16	20.6%	0.613	-8.6%
h_{st}/h_{Al}	16	25.8%	0.613	9.4%

3.3 Pattern Analysis

To systematically quantify the predictive performance of the proposed equivalent model for different material pairings and to clarify the model applicability boundaries and accuracy evolution patterns, this section summarizes the validation data for three typical target material pairing categories: aluminum-aluminum, aluminum-steel, and steel-steel. Based on Table 5, a horizontal comparative analysis is conducted from four dimensions: mean absolute percentage error, linear correlation coefficient, material ductility characteristics, and model applicability. The underlying physical mechanisms of model accuracy degradation under different conditions are elucidated, and rational guidelines for model usage are established.

Table 5 Model accuracy and applicability statistics for material pairings with different failure characteristics

Pairing type	Number of pairs	MAPE	r	Number of ductile material sides	Applicability
Al→Al	724	7.40%	0.91	2/2	Applicable
Al→St	210	15.00%	0.777	1/2	Acceptable
St→Al	210	20.60%	0.777	1/2	Use with caution
St→St	16	24.20%	0.344	0/2	Not applicable

The statistical results in Table 5 demonstrate that the model prediction accuracy exhibits a stepwise decay with respect to the material pairing type: the aluminum-aluminum pairing exhibits an average prediction error of only 7.40% with a correlation coefficient of 0.91,indicating excellent model applicability; the aluminum →steel and steel →aluminum bidirectional pairings exhibit MAPE values of 15.00% and 20.60%,respectively,placing the model in the acceptable and cautious usage ranges, respectively; the steel-steel pairing error increases to 24.20%,with the correlation coefficient dropping sharply to 0.344,rendering the model inapplicable. This accuracy evolution pattern corresponds one-to-one with the variation in the number of materials satisfying the ductile-hole-growth failure mode in each pairing, indicating that the target penetration failure mechanism is the key factor controlling the prediction accuracy of the equivalent model. The pronounced prediction asymmetry in aluminum-steel bidirectional equivalence primarily arises because for aluminum →steel conversion, the aluminum alloy conforming to ductile hole-growth serves as the reference material, and only the tested steel exhibits adiabatic shear during penetration, deviating from the cavity expansion theoretical premise, thereby constraining the error within a reasonable range. For the reverse steel →aluminum conversion, the high-strength steel prone to shear plugging is used as the reference material; the penetration resistance law of the reference material itself deviates from the theoretical assumption, and its performance deviation is fully transmitted to the equivalent conversion process, ultimately resulting in a significant increase in prediction error. This indicates that in practical ballistic equivalent calculations, materials dominated by ductile hole-growth should be preferentially selected as the reference for calculating the equivalent thickness of materials prone to adiabatic shear, avoiding reverse conversion whenever possible. From a physical mechanism perspective, the intrinsic cause of accuracy degradation is that for aluminum-aluminum pairings, both materials undergo uniform plastic hole-growth throughout the perforation process, fully conforming to the fundamental assumptions of cavity expansion theory. The cavity expansion resistance S obtained from basic material mechanical parameters accurately characterizes the ballistic performance, and the equivalent formula holds true with optimal prediction accuracy. For aluminum-steel pairings, only one side satisfies the ductile-hole-growth condition; the other side is affected by adiabatic shear, and S cannot fully capture the true penetration resistance, resulting in a modest increase in model error. For steel-steel pairings, penetration of both target plates is controlled by adiabatic shear plugging, completely violating the uniform hole-growth assumption. The parameter S no longer possesses the capability for unified characterization of cross-material equivalence, and the deviations of the resistances of the two sides from the theory are mismatched with each other, ultimately leading to a sharp drop in data correlation and a dramatic increase in prediction error. These conclusions clarify the applicability boundaries of the proposed equivalent model while providing mechanistic references for research on ballistic equivalence among high-strength steels.

4 DISCUSSION AND ANALYSIS

The experimental validation in Section 3 confirms the reliability of the equivalent formula for ductile metal equivalence and demonstrates that for aluminum-steel equivalence, the model captures the trend correctly with

moderate absolute deviations. In this chapter, experimental findings are integrated with theoretical analysis to systematically discuss the physical foundation, approximation conditions, and model comparison of the equivalent formula in three aspects.

4.1 Physical Foundation and Root Causes of Accuracy

The high predictive accuracy of the equivalent model stems fundamentally from the completeness of S as the primary resistance indicator of material ballistic resistance. The perforation resistance is defined by four independent material parameters (Y,E,n,v) and is completely characterized by the scalar S. The logarithmic strain distribution within the plastic zone causes the power-law hardening law to be naturally weighted during integration, with high-strain regions (e.g., near the cavity surface) contributing significantly and low-strain regions (e.g., near the elastic-plastic boundary) contributing relatively little. Consequently, the integration result automatically transforms into the effective average flow stress over the entire strain range, rather than the flow stress at a single point. The power-law hardening integration synthesizes the multiple parameters (Y,E,n,v) into the single characterization S, thereby filtering out parameter redundancy. The ratio form allows systematic deviations in S to cancel each other between numerator and denominator, filtering out fitting noise. The algebraic exact cancellation of $\rho_t B_0$ further filters out the uncertainty of multiple parameters. This mechanism explains why a formula incorporating only four material parameters without calibration achieves a mean absolute percentage error of 7.4% on 724 independent experimental data points.

4.2 Approximation Conditions and Applicability Range

This section systematically elucidates the applicability conditions and boundary constraints of the equivalent theory approximation from three dimensions: the mathematical premise of the theoretical approximation, the practical robustness of model accuracy, and the hierarchical criteria of applicability range, clarifying the essential relationship between mathematical assumptions and physical applicability.

Table 6 Statistical evaluation of equivalent approximation criterion parameters for typical projectile-target combinations

Projectile-target combination	h(mm)	L_{eff}(mm)	h/L_{eff}	ρ_t/ρ_p	B_0N	Λh	$\Lambda h \ll 1$?
Tungsten long rod + thin Al plate	25	~120	0.21	0.15	0.39	0.025	Strictly satisfied
Steel long rod + thin Al plate	25	~120	0.21	0.34	0.39	0.056	Satisfied
APM2 + thin Al plate	10	~22	0.45	0.34	0.39	0.12	Satisfied
APM2 + medium Al plate	30	~22	1.36	0.34	0.39	0.36	Boundary
APM2 + thick Al plate	60	~22	2.73	0.34	0.39	0.72	Nominally not satisfied

The core mathematical premise of the equivalent approximation is $\Lambda h \ll 1$, where h/L_{eff} is the ratio of target plate thickness to projectile core effective length, ρ_t/ρ_p is the target-to-projectile density ratio, and B_0N is a dimensionless coefficient related to projectile nose shape. This parameter characterizes the combined influence of target plate thickness, projectile geometry, material density, and mechanical properties on the validity of the thin-layer assumption. Its theoretical significance lies in enabling the mathematical cancellation of higher-order terms, making the equivalent approximation a first-order equivalent form.

The distribution of Λh values for typical projectile-target combinations, as shown in Table 6,indicates that this parameter covers the entire spectrum from "strictly satisfied" to "nominally not satisfied": the tungsten long rod + thin aluminum plate case with Λh=0.025 satisfies the ideal thin-layer condition; the APM2 projectile core + thick aluminum plate case with Λh=0.72 exceeds the nominal small-parameter assumption, representing a non-ideal boundary condition.

To examine the practical constraint strength of the $\Lambda h \ll 1$ condition, a stratified analysis is performed on the aluminum-aluminum pairs (n=724) according to Λh intervals, with the results presented in Table 7.

Table 7 Prediction accuracy statistics of the aluminum-aluminum equivalent model for different

Λh range	Number of pairs	MAPE	r	Bias
0.2–0.5	569	7.40%	0.894	5.10%
>0.5	155	7.50%	0.943	4.80%

The statistical results reveal that the MAPE values for the two sample groups differ by only 0.1 percentage points, and the correlation coefficient r is even higher for the thick plate conditions with Λh>0.5, indicating that the prediction accuracy of the equivalent formula approximation is insensitive to the Λh parameter.

The condition $\Lambda h \ll 1$ is not a physical boundary for the validity of the formula but rather a sufficient mathematical premise for achieving cancellation of higher-order terms. Even under the extreme boundary condition of Λh=0.72,no significant degradation in model accuracy is observed, demonstrating that the constraint strength of this condition is weaker than theoretical expectations. Therefore, the physical meaning of $\Lambda h \ll 1$ needs to be redefined: it is a mathematical tool for simplifying the theoretical derivation, rather than a rigid boundary limiting model application. As long as the core failure mechanism satisfies the requirements, the model can maintain sufficient accuracy even under conditions far exceeding the nominal parameter range.

Based on the above analysis, a hierarchical criterion for the applicability range of the equivalent formula approximation is proposed, divided from highest to lowest priority into the physical layer, mathematical layer, and geometric layer:

The fundamental condition for the theory to hold is that the target plate penetration process must be dominated by ductile hole-growth as the primary failure mechanism. Aluminum alloy materials, owing to their face-centered cubic (FCC) crystal structure and high thermal diffusivity, naturally satisfy this failure mode requirement. Armor steel materials require a yield strength greater than 1100 MPa and a strain hardening exponent greater than 0.07 to ensure a plasticity-dominated penetration process. If this condition is not satisfied, the equivalent theory is inapplicable regardless of the approximation hierarchy employed.

The first-order approximation derivation of the theory depends on the mathematical condition of the dimensionless parameter $\Lambda h \ll 1$.When this condition is satisfied, the first-order approximation can be considered a rigorous first-order equivalent form of the zeroth-order theory. The ratio h/L_{eff} of target plate thickness to projectile core effective length determines the validity of the thin-layer assumption and the choice of approximation hierarchy: when $h/L_{eff} \ll 1$, even if Λh is relatively large, the thin-layer assumption remains valid, and the zeroth-order approximation can still be employed.

4.3 Comparison of Equivalent Methods

Existing equivalent target plate formulas in the literature(Zhang J W et al.2009) all conform to a power-law structure of the form $h_B/h_A=(Y_A/Y_B)^{\gamma}$, where γ varies with projectile nose shape and requires case-by-case calibration. For engineering applications, the direct strength ratio $h_B/h_A=Y_A/Y_B$ is attempted as a reference, and its comparison with the proposed method on 724 aluminum-aluminum pairs is presented in Table 8.

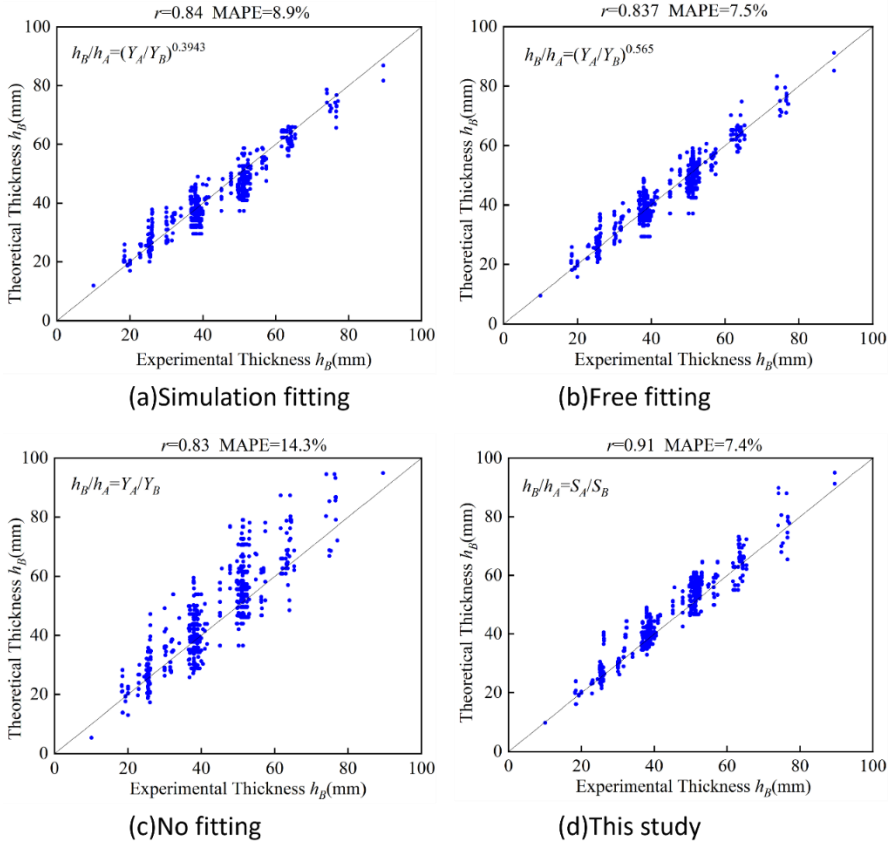

(a)Simulation fitting (b)Free fitting

(c)No fitting (d)This study

Figure 5 Comparison of Different Models

Table 8 Accuracy statistics of existing equivalent methods and the proposed S-parameter method

Method	Calibration requirement	MAPE	*r*
$h_B/h_A=(Y_A/Y_B)^{0.3943}$	Simulation fitting	8.90%	0.84
$h_B/h_A=(Y_A/Y_B)^{0.565}$	Free fitting	7.50%	0.837
$h_B/h_A=Y_A/Y_B$	No fitting	14.3%	0.83
$h_B/h_A=S_A/S_B$(this study)	No fitting	7.40%	0.91

From the data in Table 8 and Figure 5, it can be observed that traditional equivalent formulas based on the power of yield strength all require experimental/simulation fitting calibration, with correlation coefficients r concentrated in the range of 0.83–0.84. The uncalibrated pure yield strength ratio method $h_B/h_A=Y_A/Y_B$ exhibits an error as high as 14.3%, representing the poorest predictive performance. The proposed S-ratio equivalent method requires no parameter calibration, achieves a MAPE of only 7.40%, and improves the correlation coefficient to 0.91. It not only outperforms the optimally power-law fitted formula in terms of absolute prediction error but also exhibits a more pronounced advantage in trend fitting capability. Analysis reveals that the S parameter integrates multiple material properties including yield strength, strain hardening exponent, and elastic modulus, thereby providing a more comprehensive characterization of the material penetration resistance compared to traditional methods relying solely on yield strength *Y*, performing optimally under the fully ductile-hole-growth conditions of aluminum-aluminum pairs.

4.4 Cross-Category Equivalence Mechanism

The experimental results in Section 3.2 demonstrate that the MAPE for the 210 aluminum-steel pairs (15.0%–20.6%) is 2–3 times that for the 724 aluminum-aluminum pairs (7.4%), yet the trend correlation maintains *r*=0.777. Analysis reveals that the MAPE decomposed by steel type exhibits systematic differences, ranging from 4.3% for BISRHA300 to 29.7% for ARMOX560, a span of nearly sevenfold. The relationships between MAPE and two fundamental mechanical parameters of the steel—yield strength *Y* and strain hardening exponent *n*—are examined. *Y* is positively correlated with MAPE: higher *Y* tends to result in larger MAPE. *n* is negatively correlated with MAPE: at the same *Y* level, steels with higher *n* tend to exhibit lower MAPE. Figure 6 illustrates this pattern in scatter plot form.

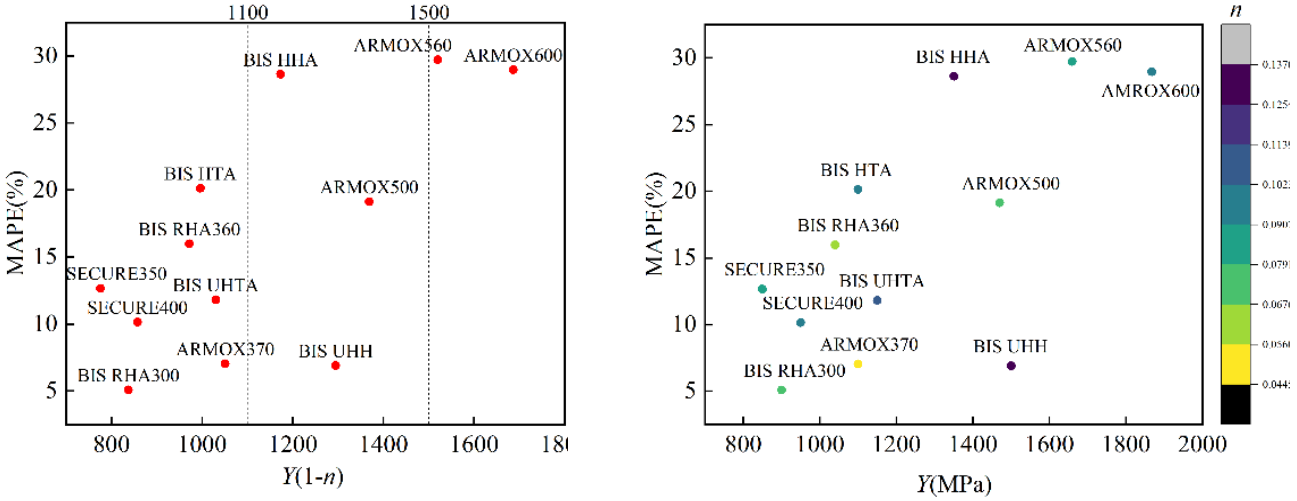

(a)*Y*(1-*n*) (b)*Y*

Figure 6 Distribution pattern of armor steel equivalent prediction error MAPE with Y(1−n) and Y

Table 9 Prediction accuracy statistics of the aluminum-aluminum equivalent model for different

Steel type	*Y*(MPa)	*n*	MAPE	*Y*(1−*n*)	Classification
BISRHA300	900	0.07	4.30%	837	Ductile hole-growth
ARMOX370	1100	0.045	7.00%	1051	Ductile hole-growth
BISUHH	1500	0.137	6.90%	1295	Ductile hole-growth (high *n* compensation)
SECURE400	950	0.097	10.40%	858	Transition zone
BISUHTA	1150	0.104	11.80%	1030	Transition zone
ARMOX500	1470	0.069	19.10%	1369	Shear-prone
ARMOX560	1659	0.084	29.60%	1520	Shear-dominated
ARMOX600	1867	0.097	28.00%	1686	Shear-dominated

To quantitatively describe the combined effect of *Y* and *n*, the composite parameter *Y*(1−*n*) is constructed, combining *Y* and (1−*n*) into a single scalar, both of which are positively correlated with MAPE. Their product amplifies the difference, indicating that it effectively captures the monotonic trend of MAPE variation. Based on the distribution in

Figure 6(a), three empirical regions can be delineated. In the region where $Y(1-n)$ <1100MPa, BISRHA300(MAPE=4.3%), ARMOX370(MAPE=7.0%), and BISUHH (MAPE=6.9%) are located, where the equivalent model accuracy approaches the aluminum-aluminum level and can be used directly. Notably, BISUHH (Y=1500MPa, n=0.137) is noteworthy: although Y is high, n=0.137 results in $1-n$=0.863, controlling the composite parameter near the threshold of 1295 MPa. In the region $1100<Y(1-n)<1500$, the accuracy of materials such as SECURE400 (MAPE=10.4%) degrades, but the trend is still maintained, allowing for preliminary screening. In the region $Y(1-n)>1500$,ARMOX560 (MAPE=29.7%) and ARMOX600 (MAPE=29.0%),the predicted values of the equivalent model deviate significantly from the experiments, and direct use is not recommended.

The above patterns are consistent with existing adiabatic shear instability theory (Bai YL, Dodd B.2009),indicating that high Y implies more heat generation per unit plastic strain, while low n implies insufficient strain hardening to maintain uniform deformation; the combination of the two tends to induce shear localization. However, this paper only provides a set of independent experimental evidence for the qualitative consistency with this theory, showing a positive correlation between $Y(1-n)$ and MAPE with r=0.90, and does not claim that the ballistic resistance of steel can be quantitatively predicted from this parameter.

5 CONCLUSIONS

Based on the Forrestal-Warren cylindrical cavity expansion penetration theory and under the condition of equal ballistic limit velocity, this paper has established and validated an armor equivalent thickness relationship that takes the power-law hardening parameters of materials (Y,E,n,ν) as inputs. The core contribution is that when the penetration inertial effect is negligible ($\Lambda h \ll 1$), the uncertain parameters (ρ_t,B_0,L_{eff},$N(\psi)$) in the original equation cancel exactly under the equivalence condition, simplifying the equivalent relationship to the form $h_B/h_A=S_A/S_B$ that depends only on the material mechanical parameters.

This method elevates armor equivalence from an empirical calibration paradigm to a physical prediction paradigm, requiring only tensile test parameters to establish cross-material equivalent relationships without the need for additional ballistic tests. Validated using 950 sets of AP armor-piercing projectile impact data, the MAPE for aluminum-aluminum equivalent thickness ratios is 7.4% with a correlation coefficient r=0.910, and aluminum-steel pairings also maintain a monotonic trend, providing a framework for first-order correction for non-ductile-hole-growth materials. This method is equivalent in physical depth to numerical solutions of cavity expansion yet requires no calibration parameters, with its accuracy surpassing all power-law models that require calibration. The ideal applicability boundary is defined by the ductile-hole-growth condition and the $\Lambda h \ll 1$ condition, and the Λh constraint can be reasonably relaxed in engineering practice to approximately 0.7 without loss of accuracy.

Author's Contribuitions: Author’ s Contributions: Investigation, Tao Li, WenJin Yao; Methodology, Tao Li, WenJin Yao; Conceptualization, Tao Li, Wei Zhu; Writing - Reviewing & Editing, Tao Li, Wei Zhu; Writing Original draft, Tao Li, Wei Zhu, Wenbin Li

Data Availability: Research data is available in a repository

Editor: Marcilio Alves

References

Bishop R F, Hill R, Mott N F. (1945). The theory of indentation and hardness tests. Proceedings of the Physical Society 57(3):147–159.

Masri R, Ryan S. (2023). Ballistic limit predictions of non-identical layered targets perforated in ductile hole formation. International Journal of Impact Engineering 171:1–12.

Masri R. (2015). Ballistically equivalent aluminium targets and the effect of hole slenderness ratio on ductile plate perforation. International Journal of Impact Engineering 80:45–55.

Qi H L, Wang X Y, Qin Y, Wen Q Y. (2024). Research on the high-speed impact of projectiles on reinforced concrete equivalent targets. Journal of Physics: Conference Series 2720:012038.

Lambert J P, Jonas G H. (1976). Towards standardization in terminal ballistics testing: velocity representation. Ballistic Research Laboratories Report, BRL-R-1852, Aberdeen Proving Ground, MD, ADA021389.

Han L, Jiang H Y. (2023). Thickness equivalent method of 921A and Q235 steel plate based on the similarity of projectile penetration residual velocity. Journal of Physics: Conference Series 2478:072028.

Wang Y N, Wang Z, Yao X L, Yang N N. (2023). Material similarity law of blunt projectiles penetrating scaled steel target plates. International Journal of Impact Engineering 178:104603.

Mullin S A, Anderson C E, Wilbeck J S. (2003). Dissimilar material velocity scaling for hypervelocity impact. International Journal of Impact Engineering 29:469–536.

Du C L, Cao J C, Qiao Y J, Zhao Z Q, Xing J, Zhang C. (2025). Rationalized equivalence method for high-velocity impacts of composite and metal panels. Composite Structures 357:118910.

Wen H M, Jones N. (1993). Experimental investigation of the scaling laws for metal plates struck by large masses. International Journal of Impact Engineering 13(3):485–505.

Du C L, Wu B W, Gao T Y, Li X, Jia Y K, Zhang C. (2025). Thickness effect and equivalency method for high-velocity impact properties of laminated composite panels. Thin-Walled Structures 217, Part B:113889.

Hill R. (1998). The mathematical theory of plasticity, Oxford University Press.

Forrestal M J, Luk V K. (1988). Dynamic spherical cavity-expansion in a compressible elastic-plastic solid. Journal of Applied Mechanics 55(2):275–279.

Luk V K, Forrestal M J, Amos D E. (1991). Dynamic spherical cavity expansion of strain-hardening materials. Journal of Applied Mechanics 58(1):1–6.

Forrestal M J, Luk V K, Brar N S. (1990). Perforation of aluminum armor plates with conical-nose projectiles. Mechanics of Materials 10:97–105.

Warren T L, Forrestal M J. (1998). Effects of strain hardening and strain-rate sensitivity on the penetration of aluminum targets with spherical-nosed rods. International Journal of Solids and Structures 35:3737–3753.

Forrestal, M.J., Warren, T.L. (2009). Perforation equations for conical and ogival nose rigid projectiles into aluminum target plates. International Journal of Impact Engineering 36(2):220–225.

Ryan, S. (2023). Ballistic limit (V50) database, Version 1, Mendeley Data.

Zhang, J.W., Wu, Z.Q., Zhang, F.C., et al. (2024). Study on Similarity and Equivalent Design Method of Steel Plate Targets with Different Materials Based on Modified Compensation Model. Acta Armamentarii 45(4):1297–1310.

Bai, Y.L., Dodd, B. (1981). A criterion for thermo-plastic shear instability. Shock Waves and High-Strain-Rate Phenomena in Metals, Plenum Press.